Supplement of Atmos. Chem. Phys., 25, 4391–4401, 2025
https://doi.org/10.5194/acp-25-4391-2025-supplement

Atmospheric Chemistry and Physics
Open Access
EGU

Supplement of

Large reductions in satellite-derived and modelled European lower-tropospheric ozone during and after the COVID-19 pandemic (2020–2022)

Matilda A. Pimlott et al.

Correspondence to: Richard J. Pope (r.j.pope@leeds.ac.uk)

Supporting Information

Introduction

This document contains supplementary text, figures and a table relevant to the methodology presented in the main manuscript. **Sections S1 – S3** and **Figures S1 – S3** provide further information about the processing of the satellite data records used in the main manuscript. **Section S4** and **Table S1** summarize the surface emission fields used in the model simulations.

Section S1

In the GOME-2B record there is an underlying negative trend in the sub-column O_3 (surface – 450 hPa) between 2015 and 2020, which is shown in **Figure S1(a)** and **(c)**. The linear trend during this period is -1.8 DU yr^{-1}. This trend is most likely due to ultraviolet (UV) degradation of the instrument. Here, we have introduced a simple correction to provide a more realistic background tendency and thus not overstate the impact of precursor emission reductions on tropospheric O_3 from COVID-19 lockdowns. **Figure S1** demonstrates the detrending methodology. Using a linear model to detrend the data creates a pattern within the record (**Figures S1(a)** and **(b)**), of very low values in 2017, increasing to 2020. This pattern was not consistent with other satellite records of lower sub-column O_3 (e.g. from IASI). The pattern suggests that the artificial trend from 2015 to 2020 is not linear, and that there is a larger negative trend between 2015 – 2017 and a smaller negative trend between 2017 – 2020. Therefore, we have used a non-linear model (2^{nd} order polynomial) to detrend the data, shown in **Figures S1(c)** and **S1(d)**. This yields a more gradual decrease in lower sub-column O_3 between 2015 and 2020, reducing the anomalous trough in 2017. The R^2 value also shows a small increase for the polynomial trend line, with 0.58, compared to 0.55 for the linear trendline. The detrended record shown in **Figure S1(d)** is added to the average O_3 across the original record, which is 16.6 DU. The detrended record used in the analysis in the main manuscript is shown in **Figure S1(e)**.

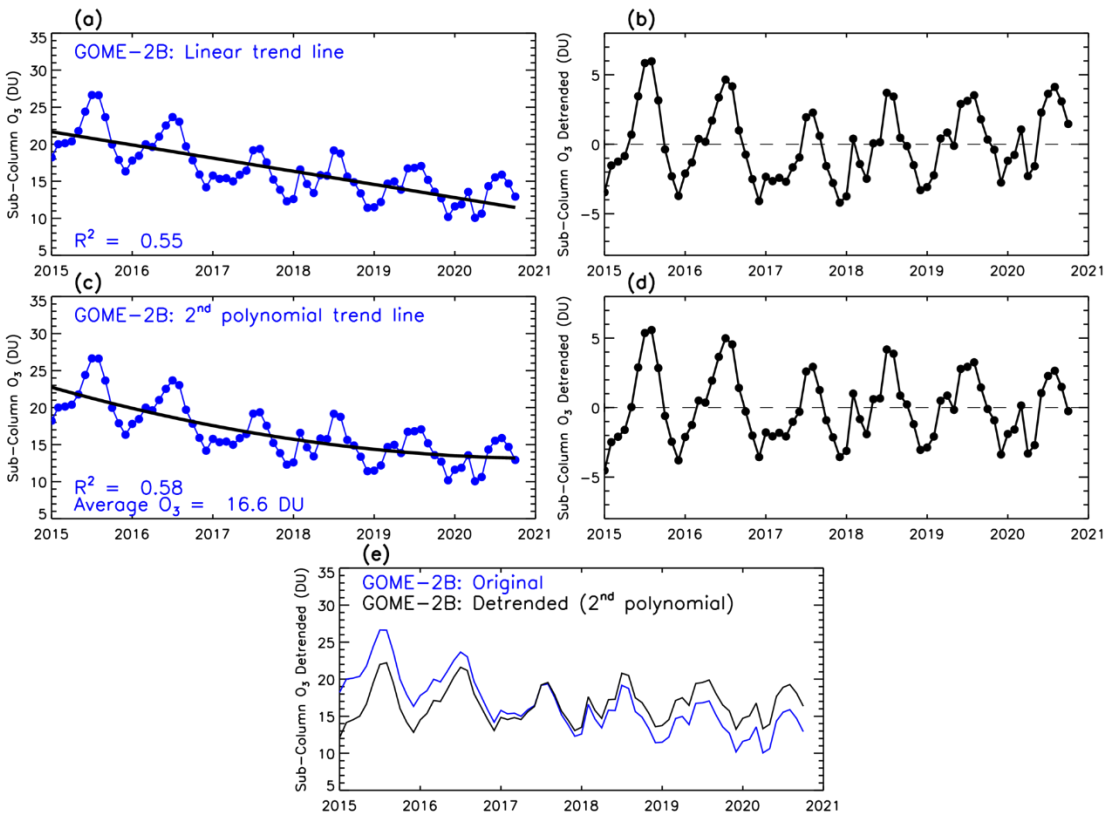

Figure S1: *Timeseries of European monthly average sub-column (surface – 450 hPa) O_3 record (DU) derived from GOME-2B between January 2015 and October 2020. (a) Original GOME-2B record for 2015 – 2020 with a linear trend line. (b) GOME-2B detrended using the linear trend model. (c) Original GOME-2B record with a 2nd-order polynomial trend line. (d) GOME-2B detrended using the 2nd-order polynomial trend model. (e) Original GOME-2B record and detrended GOME-2B record, using the 2nd-order polynomial trend model.*

Section S2

We compare satellite-derived tropospheric O_3 from IASI aboard MetOp-A and MetOp-B in the overlap year of 2018, with the aim to combine these records. **Figure S2** shows the difference between the two records for each monthly-averaged grid-box across the European domain, as used in the analysis. Across 2018, the monthly-averaged grid box differences range from -2.1 to 1.7 DU. The monthly differences show a reasonable level of consistency across the domain and therefore we have decided to adjust the monthly domain average MetOp-B record by the average difference (across the domain) between the records. **Figure S3** shows a comparison of the domain-averaged monthly records for MetOp-A and MetOp B. Broadly across 2018 MetOp-A is greater than MetOp-B

The difference ranges between -0.9 and 0.3 DU, with the largest difference in the late spring, summer and autumn months. The differences shown in **Figure S3(b)** have been subtracted from the monthly averages of all years in the MetOp-B record (2018 – 2023) to adjust for the difference.

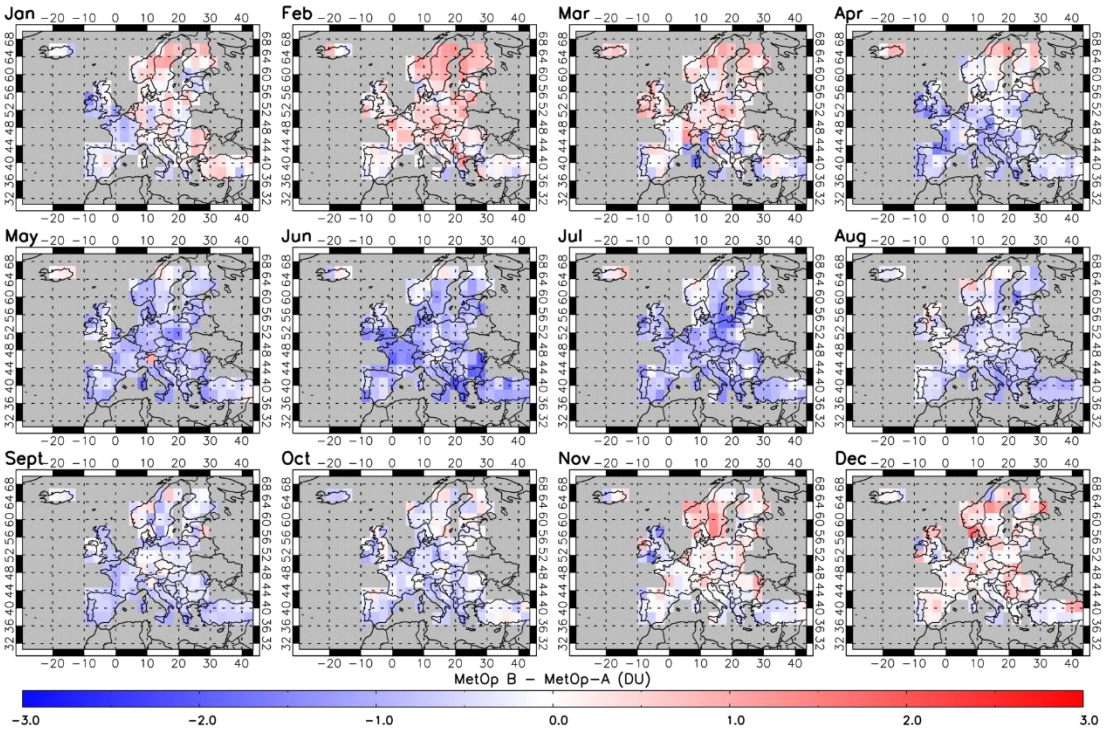

Figure S2: *Monthly difference between MetOp-A and MetOp-B (B - A) in 2018 for each grid box across the European domain used in the analysis.*

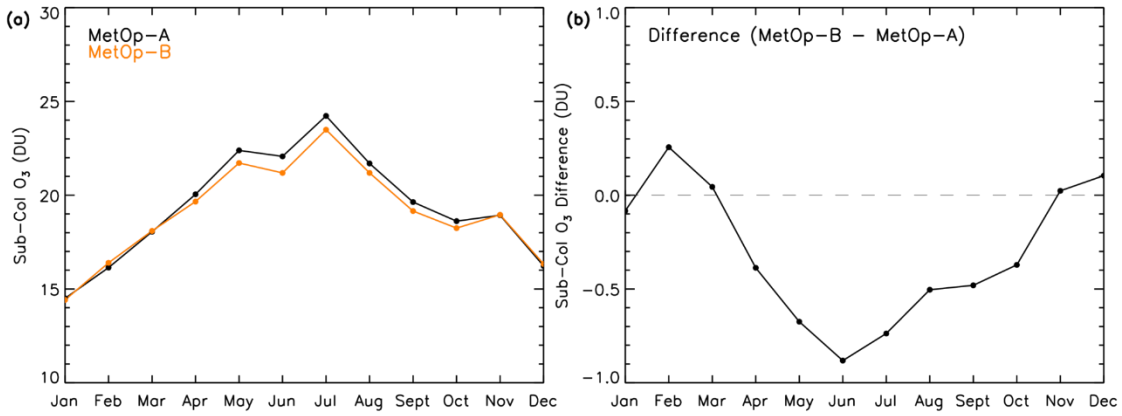

Figure S3: *Comparison of MetOp-A and B sub-column O_3 (surface – 450 hPa). (a) Monthly averages of tropospheric O_3 derived from MetOp-A and MetOp-B for all months of 2018. (b) Difference between MetOp-A and MetOp-B record (B - A).*

Section S3

The land mask used in the analysis is shown in **Figure S4**, representing the grid-boxes selected to be used in the European average calculation. The land mask was produced as part of the Hemispheric Transport of Air Pollution (HTAP) Phase 2 programme (Koffi et al., 2016) and has been interpolated onto the TOMCAT grid (2.8° × 2.8°).

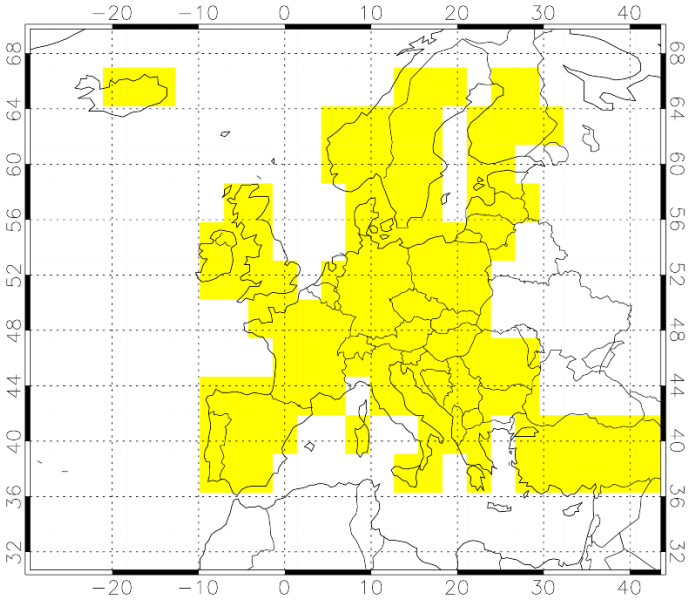

Figure S4: *Land mask used in analysis. Yellow represents the grid-boxes selected as over land.*

Section S4

The surface emission fields used in the Business-As-Usual (BAU) TOMCAT model simulation (2017 – 2021) are summarized in **Table S1**. The emissions were interpolated to a 1.0° × 1.0° grid for use in the model. The anthropogenic emissions were scaled in the COVID model simulation (2020 & 2021), as described in **Section 2.2** of the main manuscript.

Type	Description		Reference
Anthropogenic	*NO_x, CO & VOCs*	The Coupled Model Intercomparison Project Phase 6 (CMIP6) - SSP245 future emissions projections.	(Riahi et al., 2017; Gidden et al., 2019; Feng et al., 2020).
	CH_4	Emission Database for Global Atmospheric Research (EDGAR) v4.2 inventory.	(Olivier et al., 2012)
Natural (soils/ oceans)	*NO_x, CO & VOCs*	The project 'Precursors of Ozone and their Effect on the Troposphere' (POET).	(Olivier et al., 2003; Granier et al., 2005)
	CH_4	Soil sink flux comes from the Soil Methanotrophy Model (MeMo). Wetland emissions from the Joint UK Land Environment Simulator (JULES).	(Murguia-Flores et al., 2018) (Clark et al., 2011)
Biogenic	*CO & VOCs*	The Chemistry-Climate Model Initiative (CCMI) - These emissions are fixed annually.	(Morgenstern et al., 2017)
	Isoprene & monoterpenes	JULES and the UK Earth System Model (UKESM). These emissions are annually varying.	(Clark et al., 2011; Sellar et al., 2019)
Aircraft	*NO_x*	CAMS global aviation emissions (CAMS-GLOB-AIR). Used due to issues in the CMIP6 NO_x aircraft emissions between the historic emissions and the future scenario projections.	(Granier et al., 2019)
Biomass burning	*NO_x, CO & VOCs*	The Global Fire Emissions Database (GFED) version 4.	(van der Werf et al., 2017)
CH_4 scaling	Scaled to a best estimate based on the globally averaged surface CH_4 value from NOAA for each year.		(Dlugokencky, 2020)
Aerosols	*SO_2, BC & OC*	MACCity	(Granier et al., 2011)

Table S1: *Summary of surface emissions used in the TOMCAT BAU simulation for 2017 – 2021 (see **Section 2.2** of the main manuscript).*

References

Clark, D. B., Mercado, L. M., Sitch, S., Jones, C. D., Gedney, N., Best, M. J., Pryor, M., Rooney, G. G., Essery, R. L. H., Blyth, E., Boucher, O., Harding, R. J., Huntingford, C., and Cox, P. M.: The Joint UK Land Environment Simulator (JULES), model description – Part 2: Carbon fluxes and vegetation dynamics, Geosci. Model Dev., 4, 701–722, https://doi.org/10.5194/gmd-4-701-2011, 2011.

Dlugokencky, E.: NOAA Global Monitoring Laboratory – Trends in Atmospheric Methane. Available from https://gml.noaa.gov/ccgg/trends_ch4/ (accessed 1st May 2020), 2020.

Feng, L., Smith, S. J., Braun, C., Crippa, M., Gidden, M. J., Hoesly, R., Klimont, Z., van Marle, M., van den Berg, M., and van der Werf, G. R.: The generation of gridded emissions data for CMIP6, Geosci. Model Dev., 13, 461–482, https://doi.org/10.5194/gmd-13-461-2020, 2020.

Gidden, M. J., Riahi, K., Smith, S. J., Fujimori, S., Luderer, G., Kriegler, E., van Vuuren, D. P., van den Berg, M., Feng, L., Klein, D., Calvin, K., Doelman, J. C., Frank, S., Fricko, O., Harmsen, M., Hasegawa, T., Havlik, P., Hilaire, J., Hoesly, R., Horing, J., Popp, A., Stehfest, E., and Takahashi, K.: Global emissions pathways under different socioeconomic scenarios for use in CMIP6: a dataset of harmonized emissions trajectories through the end of the century, Geosci. Model Dev., 12, 1443–1475, https://doi.org/10.5194/gmd-12-1443-2019, 2019.

Granier, C., Bessagnet, B., Bond, T., D'Angiola, A., van der Gon, H.D., Frost, G.J., Heil, A., Kaiser, J.W., Kinne, S., Klimont, Z., Kloster, S., Lamarque, J.F., Liousse, C., Masui, T., Meleux, F., Mieville, A., Ohara, T., Raut, J.C., Riahi, K., Schultz, M.G., Smith, S.J., Thompson, A., van Aardenne, J., van der Werf, G.R. and van Vuuren, D.P.: Evolution of anthropogenic and biomass burning emissions of air pollutants at global and regional scales during the 1980-2010 period, Climatic Change, 109(1), 63–190, https://doi.org/10.1007/s10584-011-0154-1, 2011.

Granier, C., Darras, S., Gon, H.D. van der, Doubalova, J., Elguindi, N., Galle, B., Gauss, M., Guevara, M., Jalkanen, J.-P., Kuenen, J., Liousse, C., Quack, B., Simpson, D. and Sindelarova, K: The Copernicus Atmosphere Monitoring Service global and regional emissions (April 2019 version), https://doi.org/10.24380/d0bn-kx16, 2019.

Granier, C., Guenther, A., Lamarque, J.F., Mieville, A., Muller, J.F., Olivier, J., Orlando, J., Peters, J., Petron, G., Tyndall, G. and Wallens, S.: POET, a database of surface emissions of ozone precursors. Available from http://accent.aero.jussieu.fr/POET_metadata.php (last accessed 1st May 2020), 2005.

Koffi, B., Dentener, F., Janssens-Maenhout, G., Guizzardi, D., Crippa, M., Diehl, T. and Galmarini, S. Hemispheric Transport Air Pollution (HTAP): Specification of the HTAP2 experiments. Available from https://ec.europa.eu/jrc (last accessed 1st May 2020), 2016.

Morgenstern, O., Hegglin, M. I., Rozanov, E., O'Connor, F. M., Abraham, N. L., Akiyoshi, H., Archibald, A. T., Bekki, S., Butchart, N., Chipperfield, M. P., Deushi, M., Dhomse, S. S., Garcia, R. R., Hardiman, S. C., Horowitz, L. W., Jöckel, P., Josse, B., Kinnison, D., Lin, M., Mancini, E., Manyin, M. E., Marchand, M., Marécal, V., Michou, M., Oman, L. D., Pitari, G., Plummer, D. A., Revell, L. E., Saint-Martin, D., Schofield, R., Stenke, A., Stone, K., Sudo, K., Tanaka, T. Y., Tilmes, S., Yamashita, Y., Yoshida, K., and Zeng, G.: Review of the global models used within phase 1 of the Chemistry–Climate Model Initiative (CCMI), Geosci. Model Dev., 10, 639–671, https://doi.org/10.5194/gmd-10-639-2017, 2017.

Murguia-Flores, F., Arndt, S., Ganesan, A. L., Murray-Tortarolo, G., and Hornibrook, E. R. C.: Soil Methanotrophy Model (MeMo v1.0): a process-based model to quantify global uptake of atmospheric methane by soil, Geosci. Model Dev., 11, 2009–2032, https://doi.org/10.5194/gmd-11-2009-2018, 2018.

Olivier, J., Peters, J., Granier, C., Pétron, G., Müller, J.F. and Wallens, S. Present and future surface emissions of atmospheric compounds, POET report #2. Available from http://accent.aero.jussieu.fr/POET_metadata.php (last accessed 1st May 2020), 2003.

Olivier, J.G., Peters, J.A. and Janssens-Maenhout, G. Trends in Global CO_2 Emissions 2012 Report. Available from https://www.pbl.nl/en/publications/trends-in-global-co2-emissions-2012-report (last accessed 1st May 2020), 2012.

Riahi, K., van Vuuren, D.P., Kriegler, E., Edmonds, J., O'Neill, B.C., Fujimori, S., Bauer, N., Calvin, K., Dellink, R., Fricko, O., Lutz, W., Popp, A., Cuaresma, J.C., KC, S., Leimbach, M., Jiang, L., Kram, T., Rao, S., Emmerling, J., Ebi, K., Hasegawa, T., Havlik, P., Humpenöder, F., Da Silva, L.A., Smith, S., Stehfest, E., Bosetti, V., Eom, J., Gernaat, D., Masui, T., Rogelj, J., Strefler, J., Drouet, L., Krey, V., Luderer, G., Harmsen, M., Takahashi, K., Baumstark, L., Doelman, J.C., Kainuma, M., Klimont, Z., Marangoni, G., Lotze-Campen, H., Obersteiner, M., Tabeau, A. and Tavoni, M.: The Shared Socioeconomic Pathways and their energy, land use, and greenhouse gas emissions implications: An overview. Global Environmental Change, 42,153–168, https://doi.org/10.1016/j.gloenvcha.2016.05.009, 2017.

Sellar, A.A., Jones, C.G., Mulcahy, J.P., Tang, Y., Yool, A., Wiltshire, A., O'Connor, F.M., Stringer, M., Hill, R., Palmieri, J., Woodward, S., de Mora, L., Kuhlbrodt, T., Rumbold, S.T., Kelley, D.I., Ellis, R., Johnson, C.E., Walton, J., Abraham, N.L., Andrews, M.B., Andrews, T., Archibald, A.T., Berthou, S., Burke, E., Blockley, E.,

Carslaw, K., Dalvi, M., Edwards, J., Folberth, G.A., Gedney, N., Griffiths, P.T., Harper, A.B., Hendry, M.A., Hewitt, A.J., Johnson, B., Jones, A., Jones, C.D., Keeble, J., Liddicoat, S., Morgenstern, O., Parker, R.J., Predoi, V., Robertson, E., Siahaan, A., Smith, R.S., Swaminathan, R., Woodhouse, M.T., Zeng, G. and Zerroukat, M.: UKESM1: Description and Evaluation of the U.K. Earth System Model, Journal of Advances in Modeling Earth Systems, 11(12), 4513–4558, https://doi.org/10.1029/2019MS001739, 2019.

van der Werf, G. R., Randerson, J. T., Giglio, L., van Leeuwen, T. T., Chen, Y., Rogers, B. M., Mu, M., van Marle, M. J. E., Morton, D. C., Collatz, G. J., Yokelson, R. J., and Kasibhatla, P. S.: Global fire emissions estimates during 1997–2016, Earth Syst. Sci. Data, 9, 697–720, https://doi.org/10.5194/essd-9-697-2017, 2017.